

# Direct neutron capture cross sections of $^{62}\text{Ni}$ in the $s$ process energy range

Thomas Rauscher<sup>1</sup> and Klaus H. Guber<sup>2</sup>

<sup>1</sup>*Departement für Physik und Astronomie,*

*Universität Basel, CH-4056 Basel, Switzerland*<sup>\*</sup>

<sup>2</sup>*Nuclear Science and Technology Division,*

*Oak Ridge National Laboratory, Oak Ridge, TN 37831, USA*<sup>†</sup>

(Dated: January 29, 2020)

## Abstract

Direct neutron capture on  $^{62}\text{Ni}$  is calculated in the DWBA and the cross sections in the energy range relevant for s-process nucleosynthesis are given. It is confirmed that the thermal value of the capture cross section contains a subthreshold resonance contribution. Contrary to previous investigations it is found that the capture at higher energies is dominated by p-waves, thus leading to a considerably increased cross section at s-process energies and a modified energy dependence.

PACS numbers: 26.30.+k 25.40.Lw 26.20.+f 24.50.+g 25.40.-h

---

<sup>\*</sup>Thomas.Rauscher@unibas.ch; <http://nuastro.org>

<sup>†</sup>Current address: TÜV Energie- und Systemtechnik GmbH Baden-Württemberg, D-68032 Mannheim, Germany

The energy range of about 10 to 50 keV is relevant for neutron captures in s-process nucleosynthesis in AGB stars and type II supernovae. A large number of efforts have been undertaken to provide the necessary information on nuclear cross sections and reaction rates for neutron captures on stable nuclides as well as long-lived isotopes in s-process branchings. Nevertheless, in a number of cases only thermal cross sections are known experimentally which have been extrapolated to the energy region of interest. This is often done assuming s-wave capture. However, there are two possible sources of error in such a treatment, even in absence of resonances in the relevant energy region. Firstly, the direct capture (DC) contribution may include higher partial waves which will become increasingly important with increasing energy. Secondly, the thermal cross section may be dominated by the tail of a subthreshold resonance. In the latter case, a simple s-wave extrapolation is not justified. For neutron capture on  $^{62}\text{Ni}$  both effects are relevant. A calculation of the DC contribution can help to resolve both problems.

The two most recent recommended values of the 30 keV Maxwellian Averaged Cross Section (MACS) are  $35.5 \pm 4$  mb and  $12.5 \pm 4$  mb, as quoted by Refs. [1] and [2], respectively. A closer scrutiny shows that they are both based on the same experimental thermal neutron capture cross section but with different assumptions for the extrapolation to 30 keV [3]. In the earlier extrapolation the thermal value was taken to contain DC only which was then extrapolated assuming s-wave capture. In the more recent re-evaluation it was realized that a narrow subthreshold resonance at -0.077 keV could have contributed to the thermal value of 14.5 barn. The new extrapolation was then performed by subtracting an estimated resonance contribution and assuming s-wave DC for the remaining cross section.

This clearly shows the need for a more consistent treatment, including a more complete description of the DC process. In the following, the DC contribution to the thermal cross section is studied as well as the behavior in the range of several tens of keV.

The DC calculation was performed in a way as adopted in many other investigations (e.g. [4, 5]), making use of the code TEDCA [6], including E1, M1, and E2 transitions. See those references for more details on the DC formalism. The number of open parameters is considerably reduced by employing folding potentials for the optical potentials of target plus incident neutron and of the final neutron bound state. The folding potential is obtained by folding the projectile and target density distributions  $\rho_a$ ,  $\rho_A$  with an energy- and density-

dependent effective nucleon-nucleon interaction  $v_{\text{eff}}$  [7]

$$V(R) = \lambda V_F(R) = \lambda \int \int \rho_a(\vec{r}_1) \rho_A(\vec{r}_2) v_{\text{eff}}(E, \rho_a, \rho_A, s) d\vec{r}_1 d\vec{r}_2 , \quad (1)$$

with  $\lambda$  being a potential strength parameter close to unity, and  $s = |\vec{R} + \vec{r}_2 - \vec{r}_1|$ , where  $R$  is the separation of the centers of mass of the projectile and the target nucleus. For nucleons the density distribution is usually described by a delta function, simplifying the double integration to a single one. Often, the imaginary part of the potential is very small due to the small flux into other reaction channels and can be neglected in most cases involving neutron capture at low energies [8]. In the present case this assumption is well justified because no other reaction channels are open in the investigated energy range. The density was derived from measured charge distributions [9].

For the potential describing the final bound state of the captured neutron the parameter  $\lambda_f$  is fixed by the known binding energy. The value of  $\lambda_i$  in the entrance channel is left to be determined. This can be achieved by describing elastic neutron scattering data. In general, elastic scattering contains contributions from potential scattering and resonant scattering. Since a description of the non-resonant direct process is to be found, it is essential to use potential scattering cross sections or scattering lengths without resonant contributions. Here,  $\lambda_i$  is determined by reproducing the potential scattering length of  $6.3 \pm 0.4$  fm [10]. The experimental error can be included, leading to a range of permitted values for  $\lambda_i$  bounded by the two extremes  $\lambda_{\text{high}} = 0.81552$  and  $\lambda_{\text{low}} = 0.81392$ . Thus, there remain no open parameters in this calculation which would have to be fitted to reaction data.

Not only capture of neutrons into the ground state of  $^{63}\text{Ni}$  is relevant but also transitions to excited states have to be included. Table 1 shows the considered final states and transitions, along with the adopted spectroscopic factors and the dominating partial waves. The level scheme of  $^{63}\text{Ni}$  and the spectroscopic factors are taken from several  $^{62}\text{Ni}(\text{d},\text{p})^{63}\text{Ni}$  experiments, as usual. The spectroscopic factors are renormalization factors for each transition to a certain nuclear level, containing nuclear structure effects. The error on the spectroscopic factors is given as about 20%, therefore an additional uncertainty of 20% has been added to the error in  $\lambda_i$  arising from the scattering lengths. The relative importance of the contribution of each transition depends on the reaction  $Q$  value, the possible partial waves (s, p, d, ...-wave capture) and the spectroscopic factors. Therefore, nuclear states at high excitation energy do not contribute considerably, neither do states with small spectroscopic factors.

By far dominating are E1 s- and p-wave captures. Higher partial waves and multipolarities have been included in the calculation but as their contribution is lower by several ten orders of magnitude they are not explicitly considered in the discussion below.

The total DC cross section is the sum of all transitions to the final states. Realizing that s-, p- and d-waves are dominant, a simple parameterization of the cross section can be given:

$$\sigma = \frac{X}{\sqrt{E}} + Y\sqrt{E} + ZE^{3/2} , \quad (2)$$

with the three terms referring to transitions with orbital angular momentum  $l = 0, 1, 2$ . Including the errors derived above, the following range  $\sigma_{\text{low}} \leq \sigma \leq \sigma_{\text{high}}$  is found:

$$\sigma_{\text{high}} = 1.1 \left( \frac{2.714 \times 10^{-2}}{\sqrt{E}} + 3.85 \times 10^{-3} \sqrt{E} \right) , \quad (3)$$

$$\sigma_{\text{low}} = 0.9 \left( \frac{2.48 \times 10^{-2}}{\sqrt{E}} + 3.525 \times 10^{-3} \sqrt{E} \right) , \quad (4)$$

with the center-of-mass energy  $E$  of the incident neutron given in keV and the resulting cross section  $\sigma$  in barn. The factors before the brackets describe the uncertainty in the spectroscopic factors. In the above Eqs. 3-4 the d-wave terms are not shown because they are smaller by six orders of magnitude than the p-wave terms. With such a parameterization it is easy to disentangle the contributions from different partial waves. Contrary to previous estimates, p-wave capture dominates the cross section in the energy range relevant for s-process nucleosynthesis. Therefore, the cross section increases with energy after an initial decline, leading to a higher value at 30 keV. This contribution is entirely due to capture in the  $1/2^+$  state at  $E_x = 2.955$  MeV. This state is well established as it was seen in several experiments [11, 12, 13]. A number of  $5/2^+$  states and a  $1/2^+$  state at higher excitation energy are also reached by p-wave capture but their contributions are small due to smaller  $Q$  values and smaller spectroscopic factors.

Since potential scattering lengths were used, the derived potential should not include resonant contributions. In other words, the calculated thermal cross section of  $5.21 \pm 0.76$  barn is the purely direct contribution to the measured cross section of  $14.5 \pm 4$  barn whereas the difference is due to the high-energy tail of the subthreshold resonance plus the low-energy tails of resonances at positive energies. The DC value also fits well into the thermal cross section systematics of the other Ni isotopes which do not show subthreshold resonances.

It is quite simple to convert the above parameterization in Eq. (2) of the cross section  $\sigma$  to one describing the MACS  $\langle \sigma \rangle = \langle \sigma v \rangle / v_T$  by multiplying the p-wave term by 1.5, the

TABLE I: Transitions considered in the calculation of direct neutron capture on  $^{62}\text{Ni}$  ( $J^\pi = 0^+$ ). Shown are the states in the final nucleus  $^{63}\text{Ni}$ , the reaction  $Q$  value, contributing angular momentum  $l$  and the spectroscopic factors  $C^2S$ .

| $Q$ [MeV] | $J^\pi$                      |   | Transition |                   | $C^2S$             |
|-----------|------------------------------|---|------------|-------------------|--------------------|
| 6.838     | $\frac{1}{2}^-$              | s | →          | 2p <sub>1/2</sub> | 0.370 <sup>a</sup> |
|           |                              | d | →          | 2p <sub>1/2</sub> | 0.370 <sup>a</sup> |
| 6.751     | $\frac{5}{2}^-$              | d | →          | 1f <sub>5/2</sub> | 0.563 <sup>a</sup> |
| 6.683     | $\frac{3}{2}^-$              | s | →          | 2p <sub>3/2</sub> | 0.275 <sup>a</sup> |
|           |                              | d | →          | 2p <sub>3/2</sub> | 0.275 <sup>a</sup> |
| 6.323     | $\frac{3}{2}^-$              | s | →          | 2p <sub>3/2</sub> | 0.080 <sup>a</sup> |
|           |                              | d | →          | 2p <sub>3/2</sub> | 0.080 <sup>a</sup> |
| 5.835     | $\frac{1}{2}^-$              | s | →          | 2p <sub>1/2</sub> | 0.330 <sup>a</sup> |
|           |                              | d | →          | 2p <sub>1/2</sub> | 0.330 <sup>a</sup> |
| 5.511     | $\frac{3}{2}^-$ <sup>b</sup> | s | →          | 2p <sub>3/2</sub> | 0.125 <sup>a</sup> |
|           |                              | d | →          | 2p <sub>3/2</sub> | 0.125 <sup>a</sup> |
| 3.885     | $\frac{1}{2}^+$              | p | →          | 3s <sub>1/2</sub> | 0.190 <sup>a</sup> |
| 3.665     | $\frac{5}{2}^-$              | d | →          | 1f <sub>5/2</sub> | 0.027 <sup>a</sup> |
| 3.555     | $\frac{5}{2}^+$              | p | →          | 2d <sub>5/2</sub> | 0.036 <sup>c</sup> |
| 3.129     | $\frac{5}{2}^+$              | p | →          | 2d <sub>5/2</sub> | 0.016 <sup>c</sup> |
| 2.926     | $\frac{5}{2}^+$              | p | →          | 2d <sub>5/2</sub> | 0.027 <sup>c</sup> |
| 2.899     | $\frac{5}{2}^+$              | p | →          | 2d <sub>5/2</sub> | 0.050 <sup>c</sup> |
| 2.786     | $\frac{5}{2}^+$              | p | →          | 2d <sub>5/2</sub> | 0.070 <sup>c</sup> |
| 2.580     | $\frac{1}{2}^+$              | p | →          | 3s <sub>1/2</sub> | 0.069 <sup>c</sup> |
| 2.462     | $\frac{5}{2}^+$              | p | →          | 2d <sub>5/2</sub> | 0.032 <sup>c</sup> |
| 2.294     | $\frac{5}{2}^+$              | p | →          | 2d <sub>5/2</sub> | 0.024 <sup>c</sup> |

<sup>a</sup>Excitation energies, spins, and spectroscopic factors from [11].

<sup>b</sup>Spin assignment from [12].

<sup>c</sup>Excitation energies, spins, and spectroscopic factors from [13].

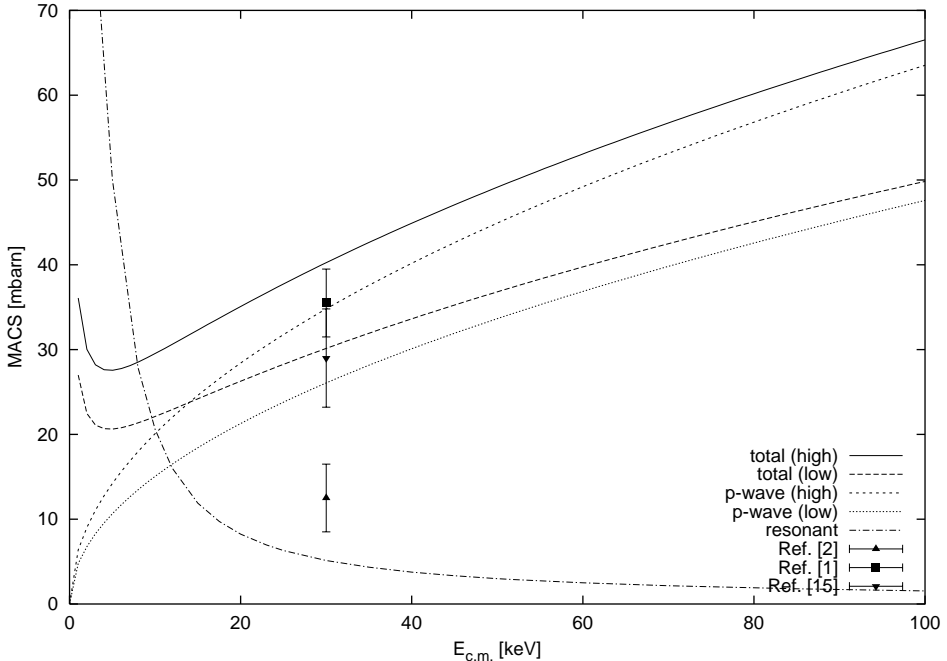


FIG. 1: MACS in the energy range  $1 \leq E_{\text{c.m.}} \leq 100$  keV. For the DC component, the upper and lower limit of the sum of all partial waves (total), and the high and low limit of the p-wave are shown. The results are compared to two values derived from thermal neutron capture data and extrapolated to 30 keV, taken from [1] and [2]. A previous experimental value from [15] is also shown. Finally, the contribution of resonant capture including several resonances and calculated from resonance parameters taken from [16] is plotted (dot-dashed line).

d-wave term by 3.75, and keeping the previous parameters, thus obtaining

$$\langle \sigma \rangle_{\text{DC}} = \frac{X}{\sqrt{E}} + 1.5Y\sqrt{E} + 3.75ZE^{3/2} . \quad (5)$$

Thus, the DC MACS is considerably enhanced when including the p-wave capture. This leads to a MACS of  $30.1 \leq \langle \sigma \rangle_{\text{DC}} \leq 40.2$  mb at 30 keV. This is back to the original value given in [1] (but for different reasons), also consistent with older data [14, 15]. The resulting MACS up to 100 keV are shown in Fig. 1.

The resonant contribution can be estimated from the resonance parameters given in literature [16] and is shown as an additional line in Fig. 1. Although this may look close to a  $1/v$  function at first glance, the behavior is not that simple because it is a sum of several resonances and the energy-dependence of the widths has been taken into account in the calculation performed with the multilevel  $R$ -matrix code SAMMY [17]. For a determination of the total rate, it has to be added to the direct terms. As can be seen from Fig. 1, the

resonant contribution is small (5.13 mb) at 30 keV. The fact that resonances are not very important at this energy is underlined by a comparison to statistical model calculations [18] which shows that the direct reaction mechanism is dominating. The level density in this nucleus is theoretically estimated to be close to the limit to allow application of the statistical model. Thus it is to be expected that any statistical model will even overestimate the actual statistical resonant cross section. Single, previously unresolved resonances could still contribute but due to the rather wide level spacing their effects might be limited because of the averaging taking place in the integration performed in the calculation of the MACS and the reaction rate. Nevertheless, a measurement in the relevant energy region is highly recommended.

Neglecting d-wave capture and utilizing the above parameterizations, the resulting astrophysical reaction rate for the direct contribution in  $\text{cm}^3 \text{ mol}^{-1} \text{ s}^{-1}$  is given by

$$N_A \langle \sigma v \rangle_{\text{DC}} = \frac{2.64545 \times 10^7}{\sqrt{\mu}} (X + 1.16045 \times 10^{-2} Y T_9) \quad , \quad (6)$$

with the reduced mass  $\mu$ , Avogadro's number  $N_A$  and the temperature  $T_9$  in  $10^9 \text{ K}$ . The constant term arises from s-wave capture, the temperature dependent term includes the p-waves. The thermal population of excited states in the target can be neglected at low temperatures. The rate (also the cross section and the MACS) is bounded by  $X_{\text{low}} = 2.232 \times 10^{-2} \text{ barn keV}^{1/2}$ ,  $Y_{\text{low}} = 3.1725 \times 10^{-3} \text{ barn keV}^{-1/2}$  and  $X_{\text{high}} = 2.985 \times 10^{-2} \text{ barn keV}^{1/2}$ ,  $Y_{\text{high}} = 4.235 \times 10^{-3} \text{ barn keV}^{-1/2}$ . This rate is a lower limit because resonant contributions are neglected. The rate obtained by fitting the resonant contribution shown in Fig. 1 has to be added to the above DC rate:

$$N_A \langle \sigma v \rangle_{\text{res}} = \exp \left( -3.80993 - \frac{0.0512461}{T_9} - \frac{1.63596}{T_9^{1/3}} + 21.4001 T_9^{1/3} - 3.29138 T_9 + 0.3822399 T_9^{5/3} - 5.52698 \ln T_9 \right) \quad . \quad (7)$$

The fit function was chosen according to the standard format as specified in [18]. The resulting total rate  $N_A \langle \sigma v \rangle = N_A \langle \sigma v \rangle_{\text{DC}} + N_A \langle \sigma v \rangle_{\text{res}}$  is valid in the temperature range  $0.001 \leq kT \leq 100.0 \text{ keV}$ .

The enhanced rate has some impact also on type II supernova nucleosynthesis. In a recent study of nucleosynthesis in type II supernovae, using an extended reaction network including all stable nuclides up to Bi [19, 20, 21], the smaller value of [2] was used. Although AGB stars are considered to be the main source of the s-process nuclides in the solar system (see

e.g. [22]), considerable s-processing also occurs in the early burning stages of massive stars producing the weak s-process component. (This component also provides seed nuclides for the  $\gamma$ -process which produces proton-rich nuclei by photo-disintegration.) In the supernova nucleosynthesis calculation an enhanced production of  $^{62}\text{Ni}$  relative to the other Ni isotopes was found (see Fig. 2 in [20] and Figs. 2–6 in [21]). Using the previous value for  $^{62}\text{Ni}(n,\gamma)^{63}\text{Ni}$  as given by [1] – being higher by about a factor of 3 – there is no such overproduction (see e.g. [23]). Using the rate proposed here in type II supernova nucleosynthesis calculations, a similar result can be expected because the new rate is – within errors – compatible with the previous value of [1].

Summarizing, the consistent treatment of the reaction  $^{62}\text{Ni}(n,\gamma)^{63}\text{Ni}$  in the DC formalism confirmed the importance of a subthreshold contribution to the thermal cross section. However, it also showed that p-wave capture is the dominating contribution to the cross sections and rates in the energy range relevant for s-process nucleosynthesis, contrary to earlier assumptions. The new rate leads to  $^{62}\text{Ni}$  abundances in type II supernovae consistent with the abundance levels of neighboring isotopes and curing a pronounced overproduction observed in some of the simulations. This underlines the fact that thermal neutron capture cross sections often cannot be simply extrapolated to the 30 keV region by assuming s-wave capture. On the other hand, the example of  $^{62}\text{Ni}$  also shows that even thermal cross sections should be evaluated including a DC analyses to disentangle resonance effects and direct contributions.

The remaining uncertainty in the cross sections can be reduced by resonance measurements in the relevant energy region to include possible effects of single resonances, by neutron scattering experiments with improved accuracy to reduce the error in the potential scattering lengths, and by activation experiments within the relevant energy region which include direct and resonant contributions simultaneously but can currently only probe the MACS at a limited number of energies. In compilations such as [2] it would also be advantageous to identify those rates which are based only on the capture of thermal neutrons or are dominated by extrapolated terms.

This work is partially supported by the Office of Environmental Management and the Office of Science, U.S. Department of Energy (contract no. DE-AC05-00OR22725 with UT-Battelle, LLC) and by the Swiss National Science Foundation (grant 2000-061822.00). T.R. acknowledges a PROFIL professorship of the Swiss NSF (grants 2124-055832.98, 2124-

067428.01).

---

- [1] Z. Y. Bao and F. Käppeler, At. Data Nucl. Data Tables **36**, 411 (1987).
- [2] Z. Y. Bao, H. Beer, F. Käppeler, F. Voss, K. Wissak, and T. Rauscher, At. Data Nucl. Data Tables **76**, 70 (2000).
- [3] H. Beer (private communication).
- [4] T. Rauscher, R. Bieber, H. Oberhummer, K.-L. Kratz, J. Dobaczewski, P. Möller, and M. M. Sharma, Phys. Rev. C **57**, 2031 (1998).
- [5] H. Herndl *et al.*, Phys. Rev. C **60**, 064614 (1999).
- [6] H. Krauss, K. Grün, T. Rauscher, and H. Oberhummer, computer code TEDCA, TU Wien (Vienna, Austria), 1992.
- [7] A. M. Kobos, B. A. Brown, R. Lindsay, and G. R. Satchler, Nucl. Phys. **A425**, 205 (1984).
- [8] H. Oberhummer and G. Staudt, in *Nuclei in the Cosmos*, edited by H. Oberhummer (Springer, Berlin, 1991), p. 29.
- [9] H. de Vries, C. W. de Jager, and C. de Vries, At. Data Nucl. Data Tables **36**, 495 (1987).
- [10] S. F. Mughabghab, M. Divadeenam, and N. E. Holden, *Neutron Cross Sections* (New York: Academic Press 1981).
- [11] T. R. Anfinsen *et al.*, Nucl. Phys. **A157**, 561 (1970).
- [12] G. A. Huttlin, S. Sen, W. A. Yoh, and A. A. Rollefson, Nucl. Phys. **A227**, 389 (1974).
- [13] P. Staub, E. Baumgartner, J. X. Saladin, H. Schär, and D. Trautmann, Helv. Phys. Acta **50**, 9 (1977).
- [14] H. Beer and R. Spencer, Nucl. Phys. **A240**, 29 (1975).
- [15] H. Beer, R. Spencer, and A. Ernst, Astron. Astrophys. **37**, 197 (1974).
- [16] Cross Section Evaluation Working Group, ENDF/B-VI Summary Documentation, Report No. BNL-NCS-17541 (ENDF-201), edited by P. F. Rose (National Nuclear Data Center, Brookhaven National Laboratory, Upton, NY, 1991).
- [17] N. M. Larson, Technical Report No. ORNL/TM-9179/R5, Oak Ridge National Laboratory, 2000 (unpublished).
- [18] T. Rauscher and F.-K. Thielemann, At. Data Nucl. Data Tables **75**, 1 (2000).
- [19] T. Rauscher, A. Heger, R. D. Hoffman, and S. E. Woosley, Nucl. Phys. **A688**, 193c (2001).

- [20] T. Rauscher, A. Heger, S. E. Woosley, and R. D. Hoffman, in Neutron Spectroscopy, Nuclear Structure, Related Topics: Proc. 9<sup>th</sup> Int. Symp. Interactions of Neutrons with Nuclei (ISINN-9) (JINR, Dubna 2001), p. 389; (astro-ph/0106289).
- [21] T. Rauscher, A. Heger, R. D. Hoffman, and S. E. Woosley, Ap. J., in press (September 2002); (astro-ph/0112478).
- [22] M. Busso, R. Gallino, and G. J. Wasserburg, Ann. Rev. Astron. Astrophys. **37**, 239 (1999).
- [23] R. D. Hoffman, S. E. Woosley, and T. A. Weaver, Ap. J. **549** (2001) 1085.